Structures, phase transitions, and magnetic properties of Co$_3$Si from first-principles calculations

Xin Zhao,[1,*] Shu Yu,[1,2] Shunqing Wu,[1,2] Manh Cuong Nguyen,[1] Cai-Zhuang Wang,[1,†] and Kai-Ming Ho[1]

[1]*Ames Laboratory, U.S. DOE and Department of Physics and Astronomy, Iowa State University, Ames, Iowa 50011, USA*
[2]*Department of Physics, Xiamen University, Xiamen 361005, China*

Co$_3$Si was recently reported to exhibit remarkable magnetic properties in the nanoparticle form [B. Balasubramanian *et al.*, Appl. Phys. Lett. **108**, 152406 (2016)], yet better understanding of this material should be promoted. Here we report a study on the crystal structures of Co$_3$Si using an adaptive genetic algorithm and discuss its electronic and magnetic properties from first-principles calculations. Several competing phases of Co$_3$Si have been revealed from our calculations. We show that the hexagonal Co$_3$Si structure reported in experiments has lower energy in the nonmagnetic state than in the ferromagnetic state at zero temperature. The ferromagnetic state of the hexagonal structure is dynamically unstable with imaginary phonon modes and transforms into a new orthorhombic structure, which is confirmed by our structure searches to have the lowest energy for both Co$_3$Si and Co$_3$Ge. Magnetic properties of the experimental hexagonal structure and the lowest-energy structures obtained from our structure searches are investigated in detail.

I. INTRODUCTION

In recent years, considerable efforts have been devoted to discovering rare-earth (RE)-free permanent magnet (PM) materials [1–9]. New RE-free PM materials with enhanced magnetocrystalline anisotropy comparable to that of RE compounds [10–12] such as Nd$_2$Fe$_{14}$B and SmCo$_5$ would be of great scientific and technological interest. Although such a goal is still far from being accomplished, much progress has been made both experimentally due to the development of advanced synthesis techniques [2–6] and theoretically because of the advances in the computational capability to predict new materials with promising magnetic properties [7–9].

Most of the studies so far have focused on materials with positive magnetocrystalline anisotropy energies (MAE) K_1, while those with negative K_1 (easy plane anisotropy) are usually ignored. Very recently, an experimental study [6] showed that Co$_3$Si, exhibiting easy-plane anisotropy in the bulk form, can have high coercivity and high saturation magnetization when prepared in the form of nanoparticles. This discovery draws new attention to the materials previously overlooked.

The high-temperature phase of Co$_3$Si has been synthesized and characterized to have a hexagonal structure with space group $P6_3/mmc$ (referred to as h-Co$_3$Si structure from here on) [13–16]. Based on experimental observations, this h-Co$_3$Si structure is stable only in a narrow temperature range of $\sim$1190 °C to 1200 °C [13]. The nanoparticle phase of Co$_3$Si was produced using nonequilibrium cluster-deposition and effective easy-axis-alignment methods [6]. It was reported to have the same crystal symmetry as h-Co$_3$Si, but the lattice parameters ($a = 4.99$ Å and $c = 4.50$ Å) are much larger along the c axis than that of the bulk h-Co$_3$Si phase ($a = 4.98$ Å and $c = 4.07$ Å) [15,16], indicating the structure of the nanoparticle phase prepared under the far-from-equilibrium conditions is different from that of the high-temperature bulk h-Co$_3$Si phase. Using density functional theory (DFT) calculations [6],

the h-Co$_3$Si structure ($a = 4.99$ Å and $c = 4.50$ Å) has been shown to exhibit an easy-plane anisotropy with a high $K_1 = -6.4$ MJ/m^3, while the Co$_3$Si nanoparticle phase was measured to have very large uniaxial anisotropy $K_1 = 4.8$ MJ/m^3. These experimental and computational results are very intriguing. However, the mechanism of the structure formation and stability and the origin of strong uniaxial magnetic anisotropy in the nanoparticle phase are still not well understood.

As a first step toward comprehensive understanding of the structure, stability, and magnetic properties of the Co-Si phases formed under the nonequilibrium conditions, in this paper we investigate the energetic stability of the crystal structures of Co$_3$Si using an adaptive genetic algorithm (AGA) and their magnetic properties using first-principles calculations. We show that the structure landscape of this simple binary system is much richer than what is shown in the equilibrium phase diagram [14], especially when the magnetic interactions are included. In particular, the h-Co$_3$Si phase is found to be unstable at zero temperature when magnetic interactions are included and transforms to a more stable structure with an orthorhombic symmetry which is obtained from the AGA search for the lowest-energy structure of Co$_3$Si (referred to as the o-Co$_3$Si structure in this work). Other group-14 element analogs to Co$_3$Si (i.e., Co$_3$C, Co$_3$Ge, and Co$_3$Sn) are also investigated.

II. COMPUTATIONAL METHODS

The adaptive genetic algorithm [17,18] used to search for the crystal structure is based on real-space cut-and-paste operations [19]. AGA combines fast structure exploration by auxiliary classical potentials with accurate energy evaluation using first-principles calculations in an iterative way to ensure the efficiency and accuracy for global structure prediction. In this scheme, auxiliary classical potentials are used for the fast exploration of the configuration space, while the structures obtained from the genetic algorithm (GA) search are evaluated by DFT calculations, and then the results are used to guide the adjustments of the auxiliary potentials. By iteratively adjusting the potential parameters, the AGA search can explore various

---

*xzhao@iastate.edu
†wangcz@ameslab.gov

local basins in the configuration space effectively to locate the globally lowest energy structure for the system with given chemical compositions.

In the AGA searches for Co_3X ($X = $ C, Si, Ge, Sn), unit cells containing up to 4 f.u. are used, and no symmetry constraints are imposed. During our GA search, the embedded-atom method (EAM) [20] is used as the auxiliary classical potential. The potential parameters for Co-Co interaction are taken from the literature [21], while the X-X and X-Co interactions are modeled by Morse functions with three adjustable parameters each. The total structure population is set to be 128 in the search, and convergence is considered to be reached when the lowest energy in the structure pool remains unchanged for 300 generations. At the end of each classical GA search, the 16 lowest-energy structures are selected to perform first-principles calculations according to the AGA procedure [17], whose energies, forces, and stress are used to adjust the parameters of the EAM potential using the POTFIT code [22]. Finally, all the selected structures are collected for higher-accuracy optimization using first-principles calculations.

First-principles calculations are carried out using spin-polarized DFT within a generalized-gradient approximation (GGA) with the VASP code [23]. The GGA exchange-correlation energy functional parameterized by Perdew, Burke, and Ernzerhof (PBE) is used [24]. The plane-wave basis is used with a kinetic energy cutoff of 400 eV. The Monkhorst-Pack scheme [25] is adopted for Brillouin zone sampling with a k-point grid of $2\pi \times 0.05$ Å^{-1} during the AGA searches. In the final structure refinements, a denser grid of $2\pi \times 0.03$ Å^{-1} is used, and the ionic relaxations stop when the forces on every atom are smaller than 0.01 eV/Å. Intrinsic magnetic properties, such as magnetic moments and MAE, are also calculated using VASP. Symmetry is switched off completely when performing the calculations including spin-orbit coupling, and a much denser k-point grid ($2\pi \times 0.016$ Å^{-1}) is used in the MAE calculations to achieve better k-point convergence. In this work, MAE is defined as the energy difference between aligning the spin along the easy (hard) axis and the hard (easy) plane, resulting in a positive (negative) value.

III. RESULTS AND DISCUSSIONS

A. Phase stabilities of Co_3Si

From our AGA searches of Co_3Si, a new orthorhombic structure with space group *Cmcm* (o-Co_3Si) was discovered to have the lowest energy. In Fig. 1(a), the convex hull for the Co-Si system is constructed by considering the previously reported structures: Co_2Si [26], $CoSi$ [27], and $CoSi_2$ [28]. It can be seen that the o-Co_3Si structure has lower energy than the experimentally observed h-Co_3Si structure, with an energy difference of about 50 meV/atom. The formation energy of the o-Co_3Si structure is very close to ($\sim$9 meV above) the tie line connecting the stable Co_2Si and hcp Co phases in the convex hull. In the following, the stabilities of the Co_3Si structures are discussed in detail.

For the h-Co_3Si structure, our calculation indicates the energy of its nonmagnetic (NM) state is 8 meV/atom lower than that of the ferromagnetic (FM) state. Based on spin-polarized DFT relaxations, the equilibrium lattice parameters
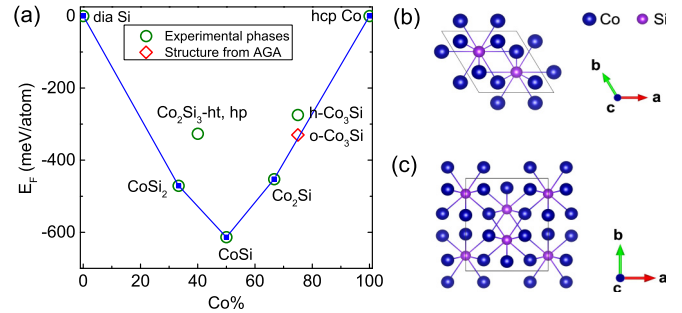

FIG. 1. (a) Formation energy convex hull of the Co-Si system. The formation energies are calculated as $E_F(Co_cSi_{1-c}) = E(Co_cSi_{1-c}) - cE(Co) - (1-c)E(Si)$, where $0 \leqslant c \leqslant 1$ and energies of the hcp Co and diamond Si are used as references. All the phases observed in experiments are indicated by green open circles, while the Co_3Si structure obtained from AGA is indicated by a red open diamond. The convex hull is constructed by the solid lines, and the stable phases based on the zero-temperature convex hulls are indicated by blue solid squares. (b) The crystal structure of the high-temperature Co_3Si phase (h-Co_3Si) observed in experiments. (c) The new lowest-energy structure (o-Co_3Si) found in our AGA searches. In (b) and (c), the bonds between Si and Co atoms are connected.

of h-Co_3Si are $a = 4.97$ Å and $c = 3.97$ Å, with the atoms occupying Co 6h (0.832, 0.664, 1/4) and Si 2c (1/3, 2/3, 1/4). However, from the nonmagnetic calculation, a slight decrease in the volume was observed: $a = 4.94$ Å and $c = 3.95$ Å, with the atoms occupying Co 6h (0.833, 0.667, 1/4) and Si 2c (1/3, 2/3, 1/4). The optimized c/a ratio (0.800) from DFT is very close to that of the bulk h-Co_3Si phase (0.817) but much smaller than that of the nanoparticle phase (0.902). For more details, in Fig. 2(a) we plot the energy of the h-Co_3Si structure as a function of volume. The data represented by solid triangles (squares) are calculated for the FM (NM) states by fully relaxing the cell shape and atom positions while keeping the volume fixed. We can clearly see that the FM state has larger equilibrium volume and higher equilibrium energy than the NM state. It is noticed that as the volume decreases, the FM state transforms to the NM state, accompanied by a sudden drop in the Co magnetic moment, as shown in the inset of Fig. 2(a). As a result, the E-V curve of the FM state (red line) jumps to overlap with that of the NM state (black line) around a volume of 9.8 Å^3/atom. The E-V relation by fixing the c/a ratio to 0.902 according to that of the nanoparticle samples was also calculated, and the results are shown as open symbols in Fig. 2(a). In this case, the FM state always has lower energy and smoothly transforms to the NM state when the volume is decreased. The FM to NM transition can also been clearly seen from the magnetic moment as a function of volume, as shown in the inset of Fig. 2(a). However, when c/a is fixed at 0.902, the energy minimum is found at a much smaller volume (10.9 Å^3/atom) compared to the value reported for nanoparticle samples (12.1 Å^3/atom) [6]. In fact, when c/a is fixed at 0.902, the equilibrium lattice constant is $a = 4.815$ Å and $c = 4.343$ Å, much smaller than those measured for the nanoparticle samples. Using the lattice constant of the Co_3Si phase in the nanoparticles proposed by experiment, the h-Co_3Si structure will have an energy 152 meV/atom higher
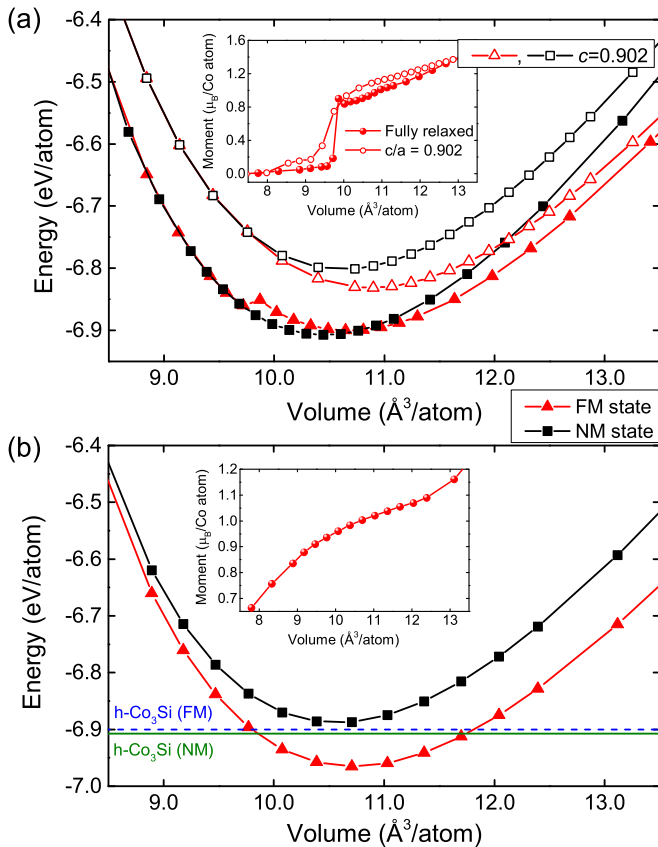
FIG. 2. Energy vs volume plot for (a) the h-Co$_3$Si structure from both fully relaxed and fixed c/a calculations; (b) the o-Co$_3$Si structure predicted from the AGA structure searches. Open symbols in (a) represent data calculated by fixing c/a to that of the nanoparticle samples, 0.902. The variation of the Co magnetic moments as a function of volume in both structures is plotted in the insets of (a) and (b).
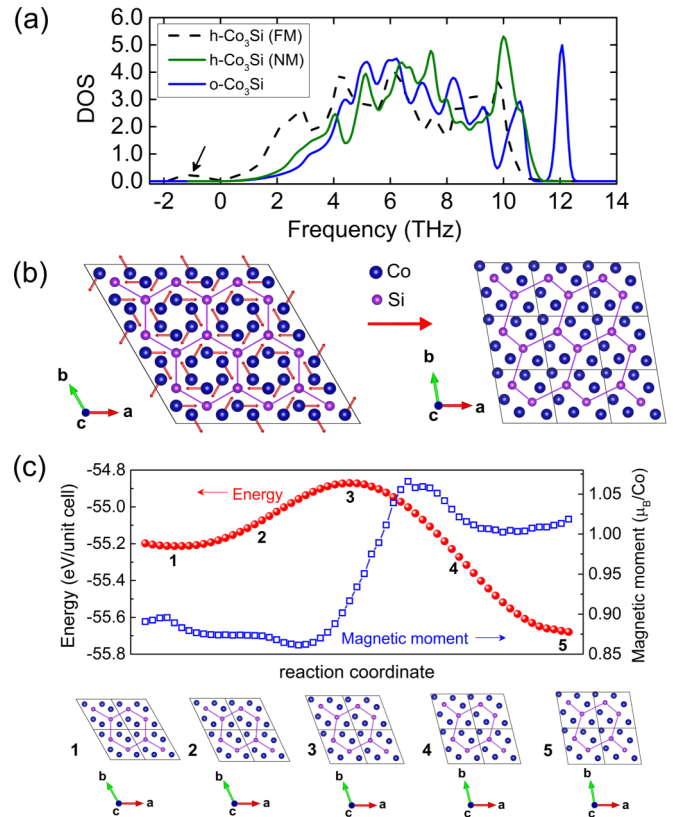

FIG. 3. (a) Phonon densities of states (DOSs) calculated for the h-Co$_3$Si structure in both NM and FM states and the o-Co$_3$Si structure in the FM state. The arrow points to the negative phonon frequencies in the FM h-Co$_3$Si structure. (b) Illustration of the structure transformation from the FM h-Co$_3$Si structure to the o-Co$_3$Si structure. The red arrows starting from the Co atoms in the h-Co$_3$Si structure indicate the eigenvectors corresponding to the imaginary phonon modes. In order to accommodate the deformation with the periodic boundary condition, the unit cell of h-Co$_3$Si is expanded by $3 \times 3 \times 1$. The o-Co$_3$Si structure plotted here is represented by its primitive cell (black boxes), with $a = b = 4.86$ Å, $c = 3.69$ Å, $\alpha = \beta = 90°$, and $\gamma = 99.69°$. Si-Si bonds are connected to guide the view. (c) Structure transition barrier calculated using the NEB method. Both the energy and magnetic moments of Co are plotted along the transition pathway. Selected structures during the transition process are presented and labeled 1 to 5.

than that of the equilibrium bulk h-Co$_3$Si phase. Although the surface effects and the synthesis procedure in the nanoparticles may contribute to stabilizing the h-Co$_3$Si structure at a lattice constant different from that of the bulk phase, it is unlikely that such effects are so strong that the lattice parameter along c can be elongated by more than 10% with an energy 152 meV/atom higher than that of the equilibrium bulk h-Co$_3$Si phase. The possibility that Co$_3$Si in the nanoparticle form may have a different atomic structure from the bulk h-Co$_3$Si phase cannot be ruled out. Further investigation to elucidate the atomic structure in the nanoparticle phase would be interesting.

The energy versus volume of the o-Co$_3$Si structure is plotted in Fig. 2(b). At equilibrium volume, its lattice parameters are $a = 6.26$ Å, $b = 7.42$ Å, and $c = 3.69$ Å, and the atoms occupy Co 8g (0.781, 0.119, 1/4), Co 4c (0.0, 0.399, 1/4), and Si 4c (0.0, 0.834, 1/4). Unlike the h-Co$_3$Si structure, there is no spin-state transition observed in the o-Co$_3$Si structure: the magnetic moment of Co atoms varies gradually with the change in volume, and the nonmagnetic state always has higher energy than the FM state. With the horizontal lines representing the energies of the h-Co$_3$Si structure in Fig. 2(b), we see that the energy of the o-Co$_3$Si structure is significantly lower than that of the h-Co$_3$Si structure.

We also computed the phonon properties of the h-Co$_3$Si and o-Co$_3$Si structures to investigate their dynamical stabilities. The phonon density of states (DOS) is calculated using a supercell approach provided by the PHONOPY code [29], where supercells with sizes of 216 atoms for the h-Co$_3$Si structure and 192 atoms for the o-Co$_3$Si structure were used. The results are plotted in Fig. 3(a). There are no negative phonon frequencies in the o-Co$_3$Si structure, indicating this structure is dynamically stable. For the h-Co$_3$Si structure, it is dynamically stable in the nonmagnetic state but shows negative phonon frequencies in the FM state, as indicated by the arrow in Fig. 3(a). It is known that the imaginary phonon modes can lead to new stable structures through atomic displacements and lattice deformation along the eigenvector of the soft mode [29]. We examined the eigenvector of the negative phonon mode and
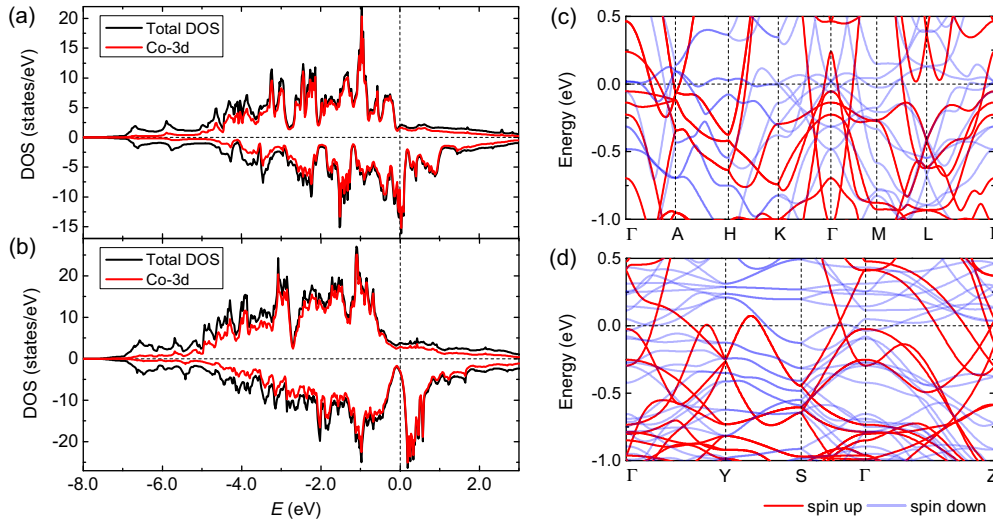
FIG. 4. (a) and (b) Electronic DOSs of the FM h-Co$_3$Si and o-Co$_3$Si structures, respectively. Both the total DOS and the contribution from Co 3d orbitals are presented. (c) and (d) Band structures of the FM h-Co$_3$Si and o-Co$_3$Si structures, respectively, along the high-symmetry k points. Fermi levels are set to zero in all plots.

found that the origin of the instability comes from the Co atoms within the Si hexagon, as shown in Fig. 3(b). The eigenvector corresponding to the imaginary phonon is plotted as the red arrows on the atoms in Fig. 3(b). By applying deformations following this eigenvector, the h-Co$_3$Si structure in the FM state can transform to the o-Co$_3$Si structure. The transformation pathway from the h-Co$_3$Si structure to the o-Co$_3$Si structure is shown in Figs. 3(b) and 3(c). Using the nudged elastic band (NEB) method [30], the transition barrier is estimated, and the results are plotted in Fig. 3(c). It can be seen that the energy barrier for the system to move from the h-Co$_3$Si structure to the o-Co$_3$Si structure is about 0.34 eV/unit cell (42.5 meV/atom). Meanwhile, along the pathway of the structure transition, there is a significant increase in the magnetic moment, from $\sim$0.88 $\mu_{\rm B}$/Co atom in the h-Co$_3$Si structure to $\sim$1.02 $\mu_{\rm B}$/Co atom in the o-Co$_3$Si structure, although the volume is only slightly increased from 10.6 to 10.7 Å^3/atom.

To further understand the origin of this phase transformation, in Fig. 4, the calculated electronic DOS and band structures are plotted and compared for the h-Co$_3$Si (FM) and the o-Co$_3$Si structures. For both structures, the DOS near the Fermi level is mainly contributed by the 3d orbitals of Co atoms, as shown in Figs. 4(a) and 4(b). It is also found that the Fermi level of the FM h-Co$_3$Si structure locates at the peak position, whereas those of the o-Co$_3$Si structures locate at the pseudogap, suggesting the phase transformation is driven by the Peierls instability [31,32]. From the band structures plotted in Figs. 4(c) and 4(d), there are fewer bands in the spin-down channel crossing the Fermi level of the o-Co$_3$Si structure than those of the h-Co$_3$Si structure, explaining the above observation in DOS.

Because the h-Co$_3$Si bulk phase can be stabilized only in a narrow high-temperature range and was reported to decompose to the Co and Co$_2$Si at lower temperatures, until now there have been no experimental studies on the magnetic properties of bulk Co$_3$Si samples. Future experiments to verify our prediction of the magnetic state of bulk h-Co$_3$Si structure at

low temperatures as well as the h-Co$_3$Si to o-Co$_3$Si structure transition would be very interesting. Based on our calculation at zero temperature, the energy of the new o-Co$_3$Si structure is more than 50 meV/atom lower than the h-Co$_3$Si structure, and the energy barrier for the proposed structure transition is estimated to be about 42.5 meV/atom, which roughly corresponds to a temperature difference of 500 K. Therefore, the o-Co$_3$Si phase should be very robust and have a high probability of being observed in experiment.

In order to gain some insight into the effect of temperature, we used quasiharmonic approximations to estimate the changes of the Gibbs free energies as a function of temperature for the different phases of Co$_3$Si with respect to Co + Co$_2$Si decomposition using the PHONOPY code [29]. Calculations were performed for all three Co$_3$Si phases, hcp Co, and Co$_2$Si at 11 different volumes to get the Helmholtz free energy as a function of the unit-cell volume. The temperature effect is taken into account via vibrational phonon entropy, where the imaginary phonon modes of h-Co$_3$Si are excluded. In addition, we note that in our calculations the magnetic moments of Co atoms are kept at zero-temperature values; that is, the magnetic phase transition was not considered automatically as temperature changes.

The results are plotted in Fig. 5. It can be seen that as the temperature increases, the free energies of NM h-Co$_3$Si and o-Co$_3$Si structures decrease much slower than that of the FM h-Co$_3$Si structure because the FM h-Co$_3$Si structure has more low-frequency phonon modes, as shown in Fig. 3(a). The free energy of NM h-Co$_3$Si is always above that of other phases. Above $\sim$850 K, the o-Co$_3$Si structure becomes the most stable phase for a narrow temperature window. The FM h-Co$_3$Si phase is estimated to have the lowest free energy above $\sim$1050 K, which is quite close to the melting temperature ($\sim$1450 K) at the composition of Co$_3$Si [14]. Note the transition temperature here can be different from the experimental observation due to the approximations used in the free-energy calculation. Despite this, the free-energy plot provides some useful insights for understanding the trends
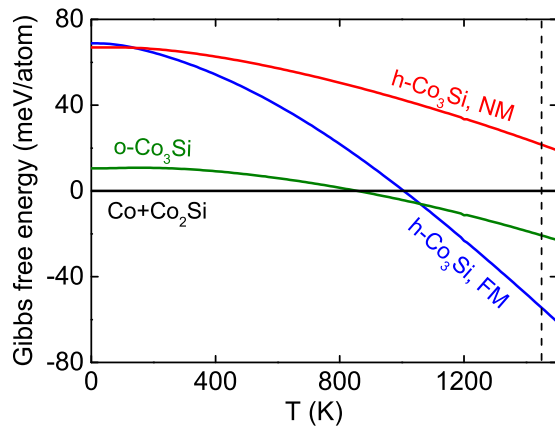
FIG. 5. Gibbs free energy of the Co_3Si structures relative to the decomposition reaction $Co + Co_2Si$ calculated from quasiharmonic approximations. The dashed vertical line represents the melting temperature of the composition of Co_3Si [14].

of phase stability at finite temperatures and could serve as a reference for the experimental synthesis effort.

B. Group-14 analogs of Co_3Si

Due to the chemical similarities among C, Si, Ge, and even Sn, it is interesting to look at the same stoichiometric compound of Co and other group-14 elements. Our crystal structure searches were also performed for Co_3X, with $X = C$, Ge, and Sn. For C or Sn, no structures were found to have

negative formation energies with respect to hcp Co and pure C or Sn diamond structure; thus, Co_3C and Co_3Sn will not be discussed in the present work.

It has been reported that Co_3Ge could exist as a stable phase at 700 °C and 750 °C, but its crystal structure remains unclear and has been speculated to have A15-type structure [14]. Our structure search demonstrated that the lowest-energy structure of Co_3Ge is the same as o-Co_3Si (referred to as o-Co_3Ge from here on). At equilibrium volume, its lattice parameters are $a = 6.43$ Å, $b = 7.55$ Å, and $c = 3.75$ Å, and the atoms occupy Co 8g (0.224, 0.116, 1/4), Co 4c (0.0, 0.400, 1/4), and Ge 4c (0.0, 0.832, 1/4). In comparison, the formation energy of the A15-type structure is positive and ~125 meV/atom higher than that of the o-Co_3Ge structure. Furthermore, the hypothetical h-Co_3Ge structure was relaxed and computed by replacing Si with Ge in the h-Co_3Si structure, but its energy in the FM state is about 51 meV/atom higher than that of the o-Co_3Ge structure. The convex hull of the Co-Ge system is constructed in Fig. 6(a), and the o-Co_3Ge structure lies below the line connecting the CoGe phase and hcp Co (~3 meV/atom below). Thus, the crystal phase observed in experiment [14] is more likely to be the o-Co_3Ge structure than the A15-type structure. Nonetheless, given that the formation energy of the room-temperature (rt) Co_2Ge phase is 6.8 meV/atom above the convex hull and it has been successfully synthesized, the experimental realization of o-Co_3Ge would be very possible.

Given the similarities between Si and Ge, the electronic properties of o-Co_3Si and o-Co_3Ge are also anticipated to
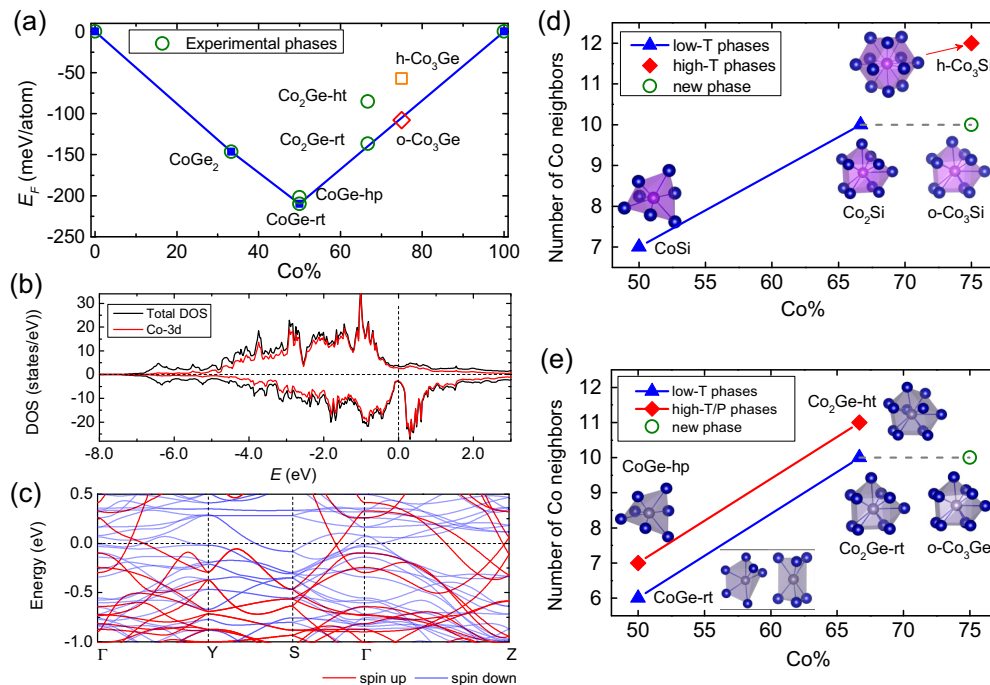

FIG. 6. (a) Formation energy convex hull of the Co-Ge system. Energies of the hcp Co and diamond Ge are used as references to calculate the formation energies. The crystal structures of the experimental phases indicated by open circles come from Ref. [33]. (b) and (c) Electronic DOS and band structure calculated for the o-Co_3Ge structure. (d) and (e) Number of neighboring Co atoms connected to Si/Ge as a function of Co composition in the known structures of Co-Si and Co-Ge systems. Blue triangles represent the low-temperature phases, and red diamonds represent the high-temperature or high-pressure phases. The new structure discovered in this work (o-Co_3X) is indicated by the green open circles. Among all the considered structures, the CoGe-rt structure has two types of Ge-centered clusters, while only one type of Si/Ge-centered cluster exists in the other structures because of their symmetries.
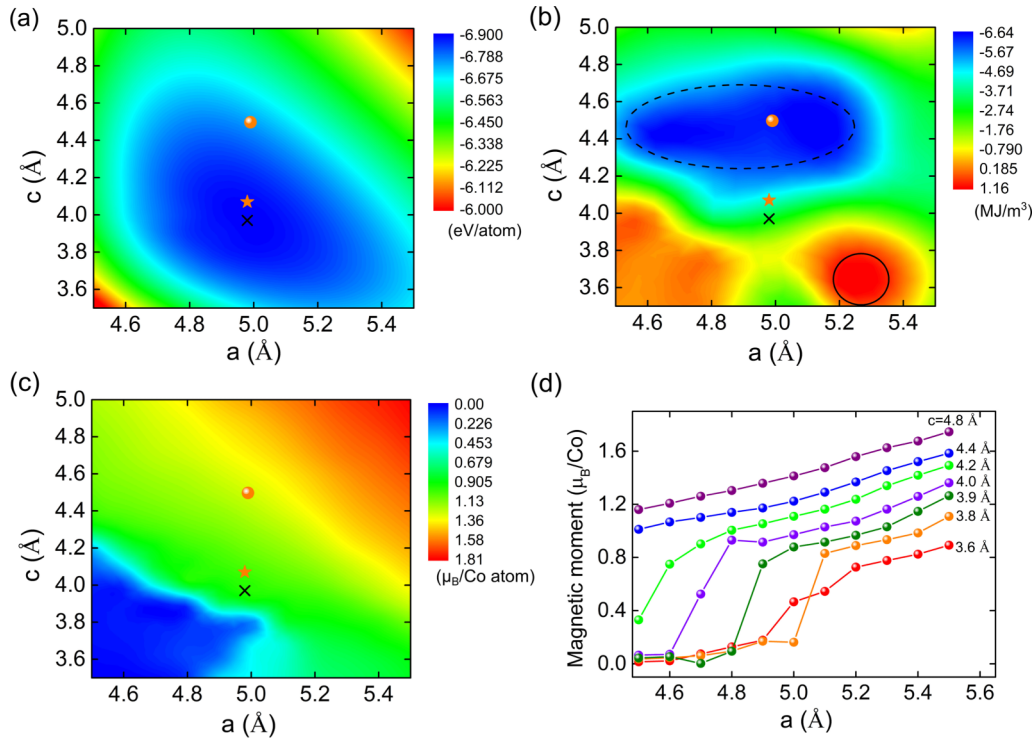
FIG. 7. Contour maps of the (a) energy, (b) magnetic anisotropy energy, and (c) Co magnetic moment of the h-Co_3Si structure as a function of its lattice parameters a and c. The star and ball represent the lattice parameters of the experimentally observed bulk sample and nanoparticle sample, respectively. The black cross represents the position of the DFT optimized lattice parameters. In (b), the black dashed circle highlights the areas with large easy-plane magnetic anisotropy, while the black solid circle highlights the areas with uniaxial magnetic anisotropy. (d) The variation of the Co magnetic moment as a function of a for fixed c.

be similar. In Figs. 6(b) and 6(c), the electronic DOS and band structure are plotted for the o-Co_3Ge structure. It can be clearly seen that both the DOS and band structure of o-Co_3Si [plotted in Figs. 4(b) and 4(d)] and o-Co_3Ge are very alike. The Fermi level of the o-Co_3Ge structure locates right at the valley around the pseudogap, indicating the stable nature of the new structure, and our phonon calculation also supports its dynamical stability by showing no imaginary frequencies.

To characterize the structures for different Co compositions in Co-Si and Co-Ge systems and understand the connections between them, we analyzed the local environment of the Si/Ge atoms in the previously reported and the newly found structures. The crystal structures of CoX, Co_2X (X = Si and Ge) are taken from the experimental studies in the literature [33]. It can already be seen from Figs. 1(b) and 1(c) that the o-Co_3X structure has very different bonding character than the h-Co_3Si structure. The h-Co_3Si structure can be considered Si-substituted hcp Co, i.e., each Si atom bonds with 12 neighboring Co atoms, while in the new structure, each Si or Ge atom bonds with 10 Co atoms, forming a distorted equatorial four-capped trigonal prism. To find the connection between the different phases, in Figs. 6(d) and 6(e), the number of neighboring Co atoms connected to Si/Ge in Co-Si and Co-Ge systems is plotted as a function of Co composition. As the Co composition is increased, more Co atoms bond with Si/Ge, as expected. We also note Si/Ge atoms in the structures observed at high temperature or high pressures tend to have more Co neighbors. In addition, it is of particular interest to see that the new o-Co_3X structure is closely related to the stable

Co_2X phases: the same Si/Ge centered cluster (XCo_{10}) is the building block for both the low-temperature Co_2X phases and the newly discovered o-Co_3X structures. In fact, there is only one type of Si/Ge centered cluster in these structures, and the different arrangements and orientations of such XCo_{10} clusters, i.e., with different amounts of face or vertex sharing, give different Co compositions.

C. Magnetic properties

As mentioned above, the Co_3Si structure synthesized in the nanoparticle form shows remarkable magnetic properties. Although the structure of this nanoparticle phase is claimed to have the same crystal symmetry as the high-temperature bulk h-Co_3Si from x-ray diffraction analysis [6], the lattice parameters and volume are very different. The volume of the bulk h-Co_3Si structure was reported to be ~ 10.9 Å^3/atom [15,16], which is rather close to the equilibrium volumes calculated by spin-polarized GGA (10.6 Å^3/atom). In the Co_3Si nanoparticles [6], the volume was reported to be 12.1 Å^3/atom. To gain a comprehensive understanding of the magnetic properties of the h-Co_3Si structure, we calculated the MAE and magnetic moments using the atomic structure from the bulk h-Co_3Si phase but varying the lattice parameters a and c. The results are summarized as contour plots in Fig. 7. First, we note again that as a varies from 4.5 to 5.5 Å and c varies from 3.5 to 5.0 Å, there is only one energy minimum at the lattice parameters close to those of the bulk h-Co_3Si phase, as plotted in Fig. 7(a).

From Fig. 7(b), we can see that MAE varies dramatically with the lattice parameters a and c. Using a and c of the nanoparticle samples, our calculation shows a MAE value of $\sim -6.1\,\text{MJ/m}^3$ ($-0.46\,\text{meV/atom}$), consistent with the previous calculation [6]. This result contradicts the experimental measurement, as has been discussed in Ref. [6], also suggesting that the crystal structure of the nanoparticle phase may be different from the bulk h-Co_3Si phase. When using the DFT optimized structure or the lattice parameters from bulk samples, the calculated MAE is much smaller, ~ -2.7 and $-3.5\,\text{MJ/m}^3$, respectively. In fact, three distinct regions can be clearly identified in Fig. 7(b): values of a and c in the left bottom corner have no magnetic anisotropy, which can be attributed to the zero magnetic moment, as shown in Fig. 7(c). Values of a and c in right bottom corner as circled by the solid black line exhibit uniaxial magnetic anisotropy ($\sim 1\,\text{MJ/m}^3$), and those in the top region circled by the dashed black line have an easy-plane magnetic anisotropy that gets as large as $-6.7\,\text{MJ/m}^3$. Here it is demonstrated again that changing the lattice parameters of the crystal structure can significantly affect the MAE, although the space-group symmetry of the crystal is fixed [34–36]. The variations of magnetic moments with a and c are plotted in Figs. 7(c) and 7(d). In general, the magnetic moment increases gradually as the unit-cell volume increases. Meanwhile, we also observed from Fig. 7(d) that for c smaller than $4.2\,\text{Å}$, there exists a sudden rise in the magnetic moment as a increases, but for $c = 4.5\,\text{Å}$ as in the nanoparticle samples, such a phenomenon does not occur.

As for the lowest-energy o-Co_3Si structure, the calculation shows that it has an easy-plane magnetic anisotropy with MAE equal to $-0.52\,\text{MJ/m}^3$, and the magnetic hard axis is along its a direction. On the other hand, the o-Co_3Ge structure, from our magnetic calculation, shows uniaxial magnetic anisotropy with the easy axis along its c direction, but its MAE is very small, $\sim 0.35\,\text{MJ/m}^3$.

IV. CONCLUSION

Our first-principles calculations on the experimentally reported hexagonal Co_3Si structure revealed a spin-state transition that has not yet been observed in experiments. At zero temperature, the h-Co_3Si structure has lower energy in the NM state than the FM state. The h-Co_3Si structure

in the FM state is dynamically unstable based on phonon calculations. With the assistance of adaptive genetic algorithm crystal structure searches, the lowest-energy structure of Co_3Si was found to be the o-Co_3Si structure with an energy $\sim 50\,\text{meV/atom}$ lower than that of the h-Co_3Si structure. A structure transformation from the ferromagnetic h-Co_3Si structure to the o-Co_3Si structure was then demonstrated, and the transition barrier was estimated to be 42 meV. Though quasiharmonic approximations, we discussed the structure evolution of the different Co_3Si phases as a function of temperature and predicted the possible temperature window to obtain new structures. By extending the study to other group-14 analogs, we showed the lowest-energy structure of Co_3Ge is the same as the o-Co_3Si structure. This o-Co_3X structure is closely related to the stable Co_2X phases in terms of the constituent structural motifs.

Magnetic properties were discussed for both the experimental and new structures of Co_3X. In order to address the effect of the different lattice parameters observed for bulk and nanoparticle Co_3Si samples on the magnetic properties, the comprehensive dependence of MAE and magnetic moments on the lattice parameters was mapped out and discussed. For the new structure, although it was found to have lower energies in both the Co-Si and Co-Ge systems, their calculated magnetic anisotropy energies are very small. Nonetheless, the proposed structure and spin transitions from the present study would provide strong motivation for devoting further experimental efforts to explore the formation of new phases under far-from-equilibrium conditions in the Co-Si and Co-Ge systems.

[1] M. J. Kramer, R. W. McCallum, I. E. Anderson, and S. Constantinides, JOM **64**, 752 (2012).

[2] T. Ogawa, Y. Ogata, R. Gallage, N. Kobayashi, N. Hayashi *et al.*, Appl. Phys. Express **6**, 073007 (2013).

[3] T. R. Gao, Y. Q. Wu, S. Fackler, I. Kierzewski, Y. Zhang *et al.*, Appl. Phys. Lett. **102**, 022419 (2013).

[4] B. Balasubramanian, B. Das, R. Skomski, W. Y. Zhang, and D. J. Sellmyer, Adv. Mater. **25**, 6090 (2013).

[5] A. M. Montes-Arango, L. G. Marshall, A. D. Fortes, N. C. Bordeaux, S. Langridge, K. Barmak, and L. H. Lewis, Acta Mater. **116**, 263 (2016).

[6] B. Balasubramanian, P. Manchanda, R. Skomski, P. Mukherjee, S. R. Valloppilly, B. Das, G. C. Hadjipanayis, and D. J. Sellmyer, Appl. Phys. Lett. **108**, 152406 (2016).

[7] E. K. Delczeg-Czirjak, A. Edstrom, M. Werwinski, J. Rusz, N. V. Skorodumova, L. Vitos, and O. Eriksson, Phys. Rev. B **89**, 144403 (2014).

[8] X. Zhao, C. Z. Wang, Y. X. Yao, and K. M. Ho, Phys. Rev. B **94**, 224424 (2016).

[9] X. Zhao, L. Q. Ke, C. Z. Wang, and K. M. Ho, Phys. Chem. Chem. Phys. **18**, 31680 (2016).

[10] M. Sagawa, S. Fujimura, N. Togawa, H. Yamamoto, and Y. Matsuura, J. Appl. Phys. **55**, 2083 (1984).

[11] R. H. J. Fastenau and E. J. van Loenen, J. Magn. Magn. Mater. **157-158**, 1 (1996).

[12] S. Sugimoto, J. Phys. D **44**, 064001 (2011).

[13] K. Ishida, T. Nishizawa, and M. E. Schlesinger, J. Phase Equilib. **12**, 578 (1991).

[14] H. Enoki, K. Ishida, T. Nishizawa, J. Less-Common Met. **160**, 153 (1990).

[15] W. Koster, H. Warlimont, and T. Godecke, Z. Metallkd. **64**, 399 (1973).

[16] L. Zhang, Y. Du, H. Xu, and Z. Pan, CALPHAD Comput. Coupling Phase Diagrams Thermochem. **30**, 470 (2006).

[17] S. Q. Wu, M. Ji, C. Z. Wang, M. C. Nguyen, X. Zhao, K. Umemoto, R. M. Wentzcovitch, and K. M. Ho, J. Phys. Condens. Matter **26**, 035402 (2014).

[18] X. Zhao, M. C. Nguyen, W. Y. Zhang, C. Z. Wang, M. J. Kramer *et al.*, Phys. Rev. Lett. **112**, 045502 (2014).

[19] D. M. Deaven and K. M. Ho, Phys. Rev. Lett. **75**, 288 (1995).

[20] M. S. Daw and M. I. Baskes, Phys. Rev. B **29**, 6443 (1984).

[21] X. W. Zhou, R. A. Johnson, and H. N. G. Wadley, Phys. Rev. B **69**, 144113 (2004).

[22] P. Brommer and F. Gahler, Modell. Simul. Mater. Sci. Eng. **15**, 295 (2007); Philos. Mag. **86**, 753 (2006).

[23] G. Kresse and J. Furthmuller, Comput. Mater. Sci. **6**, 15 (1996); Phys. Rev. B **54**, 11169 (1996).

[24] J. P. Perdew, K. Burke, and M. Ernzerhof, Phys. Rev. Lett. **77**, 3865 (1996).

[25] H. J. Monkhorst and J. D. Pack, Phys. Rev. B **13**, 5188 (1976).

[26] S. Geller and V. M. Wolontis, Acta Crystallogr. **8**, 83 (1995).

[27] J. Teyssier, R. Viennois, J. Salamin, E. Gianini, and D. Van Der Marel, J. Alloy. Compd. **465**, 462 (2008).

[28] F. Weitzer and J. C. Schuster, J. Solid State Chem. **70**, 178 (1987).

[29] A. Togo and I. Tanaka, Scr. Mater. **108**, 1 (2015).

[30] G. Henkelman and H. Jonsson, J. Chem. Phys. **113**, 9978 (2000); D. Sheppard, P. Xiao, W. Chemelewski, D. D. Johnson, and G. Henkelman, *ibid.* **136**, 074103 (2012).

[31] R. E. Peierls, *Quantum Theory of Solids* (Oxford University Press, Oxford, 1955).

[32] J. H. Xu and A. J. Freeman, Phys. Rev. B **41**, 12553 (1990).

[33] PAULING FILE, in *Inorganic Solid Phases*, edited by P. Villars, SpringerMaterials (Springer, Heidelberg, 2012).

[34] O. Hjortstam, K. Baberschke, J. M. Wills, B. Johansson, and O. Eriksson, Phys. Rev. B **55**, 15026 (1997).

[35] T. Burkert, L. Nordstrom, O. Eriksson, and O. Heinonen, Phys. Rev. Lett. **93**, 027203 (2004).

[36] A. Asali, P. Toson, P. Blaha, and J. Fidler, IEEE Trans. Magn. **50**, 7027504 (2014).